

How attractive is a barchan dune?

To cite this article: Christopher Groh *et al* 2009 *New J. Phys.* **11** 023014

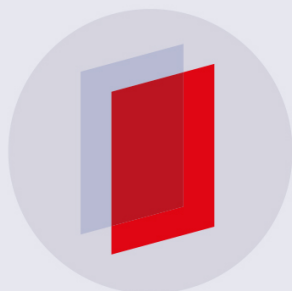
View the [article online](#) for updates and enhancements.

Related content

- [Particle dynamics of a cartoon dune](#)
Christopher Groh, Ingo Rehberg and Christof A Kruehle
- [The physics of wind-blown sand and dust](#)
Jasper F Kok, Eric J R Parteli, Timothy I Michaels *et al.*
- [The shape of barchan dunes](#)
Klaus Kroy, Sebastian Fischer and Benedikt Obermayer

Recent citations

- [Numerical Simulation of the Temporal Evolution of a Three Dimensional Barchanoid Dune and the Corresponding Sediment Dynamics](#)
M. Burkow and M. Griebel
- [Distribution of compaction bands in 3D in an aeolian sandstone: the role of cross-bed orientation](#)
Shang Deng and Atilla Aydin
- [A process-based hypothesis for the barchan-parabolic transformation and implications for dune activity modelling](#)
Thomas E. Barchyn and Chris H. Hugenholtz



IOP | ebooks™

Bringing you innovative digital publishing with leading voices to create your essential collection of books in STEM research.

Start exploring the collection - download the first chapter of every title for free.

How attractive is a barchan dune?

Christopher Groh¹, Ingo Rehberg¹ and Christof A Kruelle^{1,2}

¹ Experimentalphysik V, Universität Bayreuth, D-95440 Bayreuth, Germany

² Maschinenbau und Mechatronik, Hochschule Karlsruhe —Technik und Wirtschaft, D-76133 Karlsruhe, Germany

E-mail: Christopher.Groh@uni-bayreuth.de

New Journal of Physics **11** (2009) 023014 (13pp)

Received 29 September 2008

Published 6 February 2009

Online at <http://www.njp.org/>

doi:10.1088/1367-2630/11/2/023014

Abstract. The spatio-temporal behaviour of barchan dunes is investigated experimentally with downsized longitudinal barchan dune slices generated in a narrow water flow tube. The development towards a shape attractor is shown on the basis of four different starting configurations in qualitative observation and quantitative analysis.

Dunes, as a macroscopic manifestation between the interplay of granular matter and the flow of the surrounding fluid, are best investigated in the desert: there are definitions for star dunes, dome dunes, transverse dunes, longitudinal dunes, parabolic dunes, barchan dunes and some mixed forms [1]. A barchan dune, as shown in figure 1, has a crescent-shaped form with two horns pointing downwind.

Barchan dunes have some specific properties, which make them particularly accessible for experimental and theoretical investigations. One of their advantages is their relatively fast and simple dynamics. In fact, they are the fastest migrating dunes. This makes them traceable, because the time scale of dune migration—centuries for star dunes [2]—reduces to years. Barchan dunes exist on bedrock where the sand cover is slight. Sometimes they form barchan dune fields interacting with each other by exchanging sand [3]. But they can also exist as a single barchan dune without any immediate neighbours, a fact which often guides the theoretical modelling.

Another advantage is the weak lateral coupling of the dynamics across the wind direction. Therefore, models for barchan dunes can be cut into longitudinal slices. These infinitesimally small transverse dunes can be described with two-dimensional ‘minimal models’ [4]–[7]. These models combine an analytical description of the turbulent shear flow over low elevations [8, 9] with a continuum description, which models the saltation on the surface of the dune [10]. The model parameters have been determined by field studies [11]–[13], wind tunnel experiments [14] or, in recent times, with data taken from the surface of Mars [15, 16].

Laboratory experiments dealing with three-dimensional barchan dunes in air [17] are reproducible in experiments under water [18]–[21]. Here, the subaqueous dunes are smaller than the aeolian dunes [4, 10, 15, 17], [20]–[25], but a comparison of the morphological and dynamical properties of these dunes to field data is possible. In addition, the time scale becomes smaller: the years required to observe barchan dynamics in nature reduce to minutes or even seconds for the measurements on a lab scale.

Qualitative observations of single barchan dunes with variable experimental conditions [15, 26] or of the interaction between barchan dunes in experiments [18] and simulations [27] indicate the existence of shape attractors. Some recent models and simulations dealing with the shape attraction of barchan dunes are based on minimal models, which means that they deal with two-dimensional slices parallel to the wind direction [24, 28]. Therefore, it seems reasonable to make a retrograde step in the complexity of the corresponding experiments and to investigate the shape dynamics of intrinsically two-dimensional barchan dunes in a narrow water flow tube [29].

A sketch of our experimental setup is shown in figure 2. The main part consists of a closed flow tube, which is filled with distilled water. The lower part of the tube and the corresponding lid are machined from perspex. The height of the channel is 60 mm and its width is 50 mm. The length of the straight section is 600 mm and the curves have an outer diameter of 500 mm. The water flow is actuated by a propeller with a diameter of 45 mm, which is installed in the right curve. The propeller is driven by a motor with a shaft, which is placed in the middle of the channel profile. The flow direction is counterclockwise.

We limit the section of measurements to approximate two-dimensional conditions, comparable to a Hele–Shaw cell. Therefore, we use a black plastic insert, which constricts the channel to a width $w = 6$ mm. The aspect ratio of width to height is 10.

For the calculation of the Reynolds number Re of the 6 mm wide gap, we measure the flow velocity v_{flow} with an ultrasonic Doppler velocimeter (*Signal Processing SA*) and use the kinematic viscosity $\nu = 1 \text{ mm}^2 \text{ s}^{-1}$ of water at a temperature of 21.7 ± 0.6 °C. For the following investigations, the flow velocity is kept at $v_{\text{flow}} = 0.45 \text{ m s}^{-1}$, which corresponds to $Re = v_{\text{flow}} w / \nu = 27\,000$.

After the flume is filled with distilled water, glass beads are poured into the channel. The glass beads have a density of $\rho = 2.5 \text{ g cm}^{-3}$ and a diameter ranging 560–600 μm . The masses m of the barchan dunes are determined with an error of ± 0.005 g by weighing the glass beads. The overall mass in each sequence remains constant and amounts to $m = 16.25$ g.

In table 1, we provide characteristic numbers for the subaqueous dunes in our experiment, and list those for aeolian dunes in the desert as reported by Bagnold [3] and Finkel [30] for comparison. The velocity gradient $du_c(z)/dz$ at the onset of grain motion yields the critical shear-velocity and, subsequently, the critical particle Reynolds number and the critical Shields parameter [31]. We also calculate the dune Reynolds number with the dune height H and the particle densimetric Froude number [32], as well as the time a dune needs to migrate along its own basis length (turnover time).

A charge-coupled device (CCD) camera (*Lumenera Lw11059*) with a horizontal resolution of 4008×2672 pixels and a maximum frame rate of 5 fps is used for the measurements. The camera is placed in front of the straight part of the channel and records side views of the glass bead heaps, and the developing barchan dunes, respectively, as shown in figure 3.

The temporal evolution of the two-dimensional barchan in figure 3 starts from a triangular steep heap prepared with a funnel having a 6 mm long slit. Immediately after the propeller starts

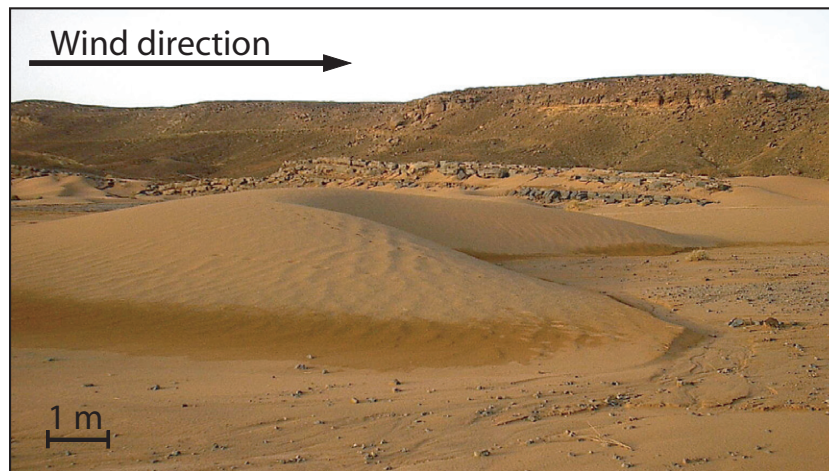


Figure 1. Photo of a barchan dune (Erfoud, Morocco).

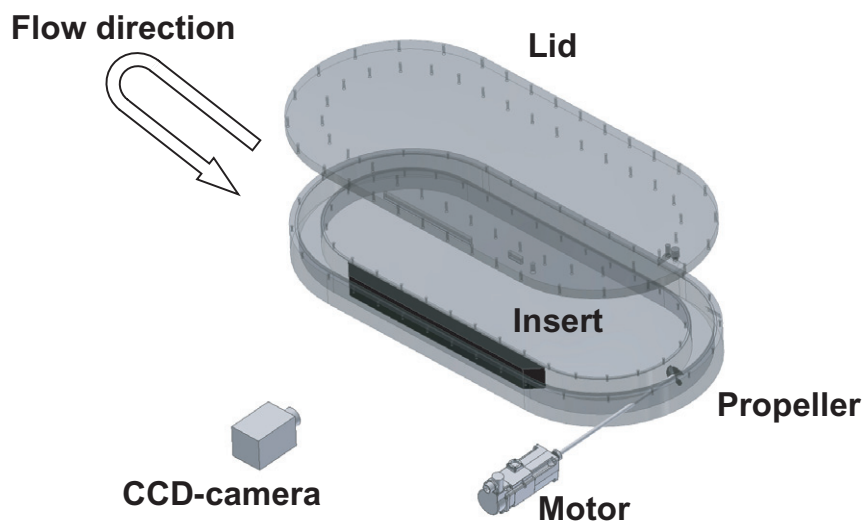


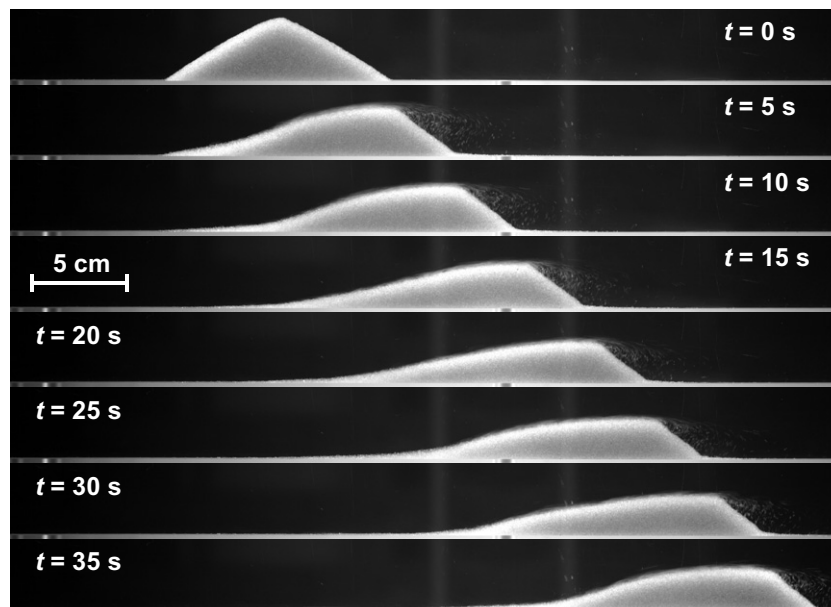
Figure 2. Sketch of the experimental setup.

and the water is actuated, the glass beads move. On the windward side, the beads are blown over the crest to the lee side, the so-called slipface, where little avalanches appear. This is the basic form of motion for the barchan dunes in our experiment, similar to the barchan dunes found in nature [17].

During the time of measurements the heap becomes lower and longer. After about 15 s its shape reaches its steady-state form. This is the attractor for $m = 16.25$ g and $Re = 27\,000$. It has been shown that the velocity takes a constant value instantaneously and mass conservation is maintained all the time. Moreover, the relaxation time towards the attractor increases with mass and decreases with the flow velocity of the overlaying water flow [29]. Note that our boundary conditions imply that the dune cannot gain sand, although it might very well lose sand.

Table 1. Comparison between subaqueous and aeolian dunes.

| | Subaqueous dunes | Aeolian dunes |
|---|---------------------------------|----------------------------------|
| Flow velocity v_{flow} | 0.5 m s^{-1} | 5 m s^{-1} |
| Critical shear-velocity $u_c^* = \sqrt{\nu \frac{du_c(z)}{dz}} _{\text{bottom}}$ | 1 cm s^{-1} | 25 cm s^{-1} |
| Mean grain diameter \bar{d} | 0.58 mm | 0.3 mm |
| Kinematic viscosity ν | $1 \text{ mm}^2 \text{ s}^{-1}$ | $15 \text{ mm}^2 \text{ s}^{-1}$ |
| Grain density ρ_g | 2.5 g cm^{-3} | 2.7 g cm^{-3} |
| Fluid density ρ_f | 1 g cm^{-3} | 1.225 mg cm^{-3} |
| Specific density $s = \rho_g/\rho_f$ | 2.5 | 2200 |
| Dune height H | 2 cm | 3 m |
| Dune basis length L | 10 cm | 20 m |
| Critical particle Reynolds number $Re_c = u_c^* \bar{d} / \nu$ | 5.8 | 5 |
| Critical Shields parameter $\Theta_c = u_c^{*2} / (g(s-1)\bar{d})$ | 0.012 | 0.010 |
| Dune Reynolds number $Re_d = v_{\text{flow}} H / \nu$ | 1×10^4 | 1×10^6 |
| Particle densimetric Froude number $Fr_p = u_{\text{flow}} / \sqrt{g(s-1)\bar{d}}$ | 5.4 | 2 |
| Migration speed v_{mig} | 1 cm s^{-1} | 20 m a^{-1} |
| Turnover time $t_t = L / v_{\text{mig}}$ | 10 s | 1 a |

**Figure 3.** Eight time sequenced snapshots show side views of a developing barchan dune slice. The glass beads appear white in front of a dark background.

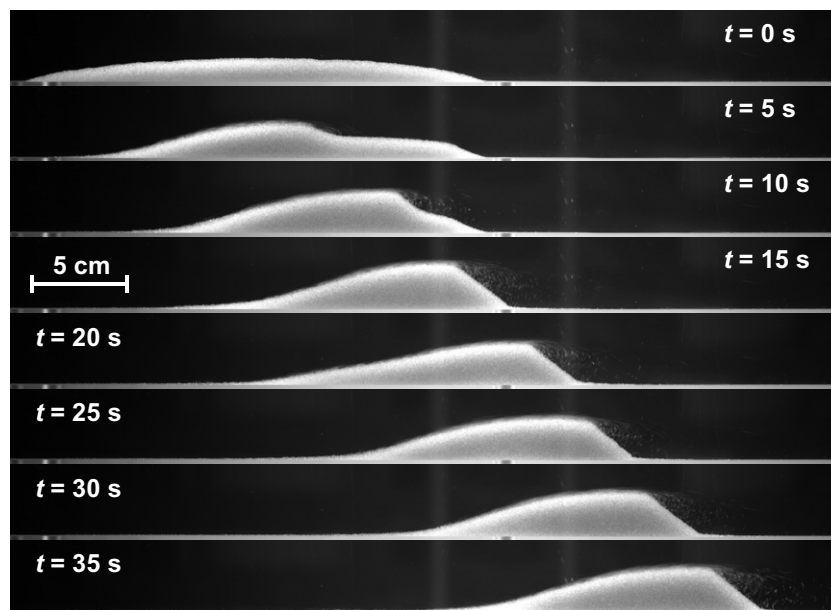


Figure 4. The development of a flat heap as start configuration shown in analogy to figure 3.

The height of the steep heap is higher than the height of its steady state. In contrast to this scenario, we prepare a flat heap with the same mass and an initial height below its steady-state value. The temporal evolution of this flat heap is shown in figure 4. The overlaying water flow pushes the growing barchan dune over the beads resting on the ground until all beads are captured. After 15 s the dune moves with constant velocity, as indicated by figure 13. At this time, the barchan dune has adopted its steady-state shape.

From the pictures in figures 3 and 4, the height profiles of the barchans are extracted by finding the lowest gradient from dark to bright. The centroid of the shape enclosed by the border line indicates the centre of mass of the barchan dune by assuming a homogeneous density distribution.

Using the centres of mass, we can perform a qualitative and quantitative comparison between the temporal evolution of the steep heap and the flat heap. For comparison, we use the centre-of-mass system as reference frame. Within this frame we place the height profiles on top of each other. The resulting figures are shown in figure 5. The corresponding movie (movie 1, available from stacks.iop.org/NJP/11/023014/mmedia) illustrates the temporal evolution for the first 35 s until the steady state is achieved.

The difference between the steep heap and the flat heap is their different starting shape, but they have the same mass of glass beads at the beginning. In order to vary the starting configuration more dramatically, we accomplish a collision between two different sized barchan dunes.

Smaller dunes are faster than larger ones [29]. Thus, we prepare a steep heap with $m = 13$ g and a smaller heap with $m = 3.25$ g in front of its windward side as shown in figure 6. If the two heaps are set in motion, the smaller heap follows the larger one, thus we refer to it as the ‘small trailer’ configuration. All other parameters are the same as in the experiments with the steep heap and the flat heap (figures 3 and 4).

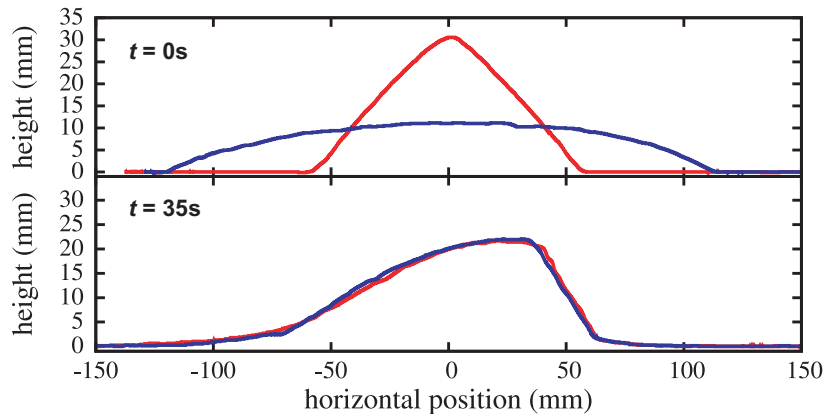


Figure 5. Height profiles of two different starting configurations (see figure 3 (red) and figure 4 (blue), $t = 0$ s) and their final steady state shapes after $t = 35$ s. The origin of the x -axis is placed in the centre-of-mass system of the barchan dunes (see movie 1, available from stacks.iop.org/NJP/11/023014/mmedia).

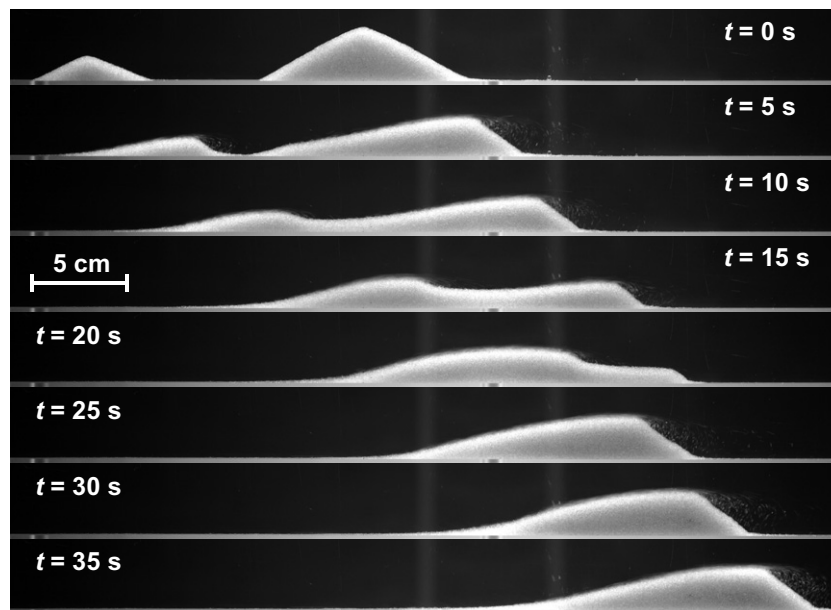


Figure 6. The development of the ‘small trailer’ as start configuration shown in analogy to figure 3.

The temporal evolution of the small trailer is shown in figure 7 as a stack plot of the height profiles. At the beginning, the scenario is the same as that for the single steep heap in figure 3. The shapes of two heaps develop to their attractor and the arising barchan dunes move with constant migration velocity in the flow direction. After about $t = 7$ s, the faster smaller barchan reaches the larger one. Between $t = 20$ s and $t = 25$ s the rest of the large heap stops because it lies in the slipstream of the growing former small barchan dune. At $t = 25$ s, the two barchans coalesce and a new barchan dune with a mass of $m = 16.25$ g is formed.

One might assume that if the small heap is placed in the flow direction behind the large heap, the developed faster small barchan dune can escape. But this is only the case if the distance

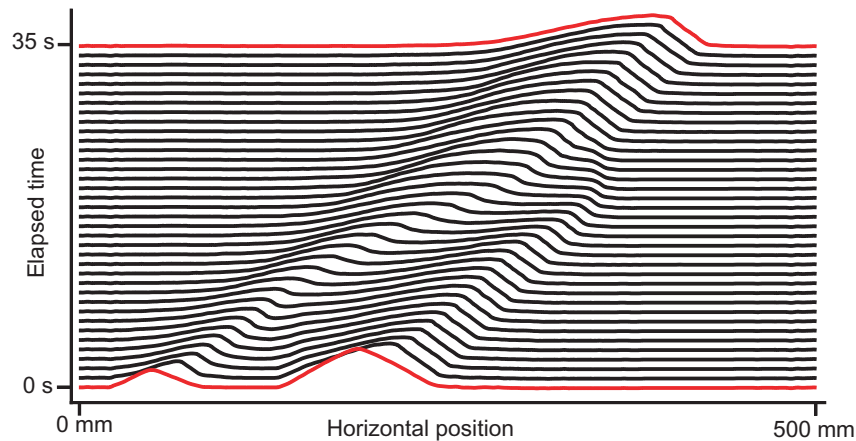


Figure 7. Temporal evolution of the height profile of the small trailer (see figure 6) is shown as stack plot. The time step between each line is 1 s. The starting profile and the final profile are marked red (see movie 2, available from stacks.iop.org/NJP/11/023014/mmedia).

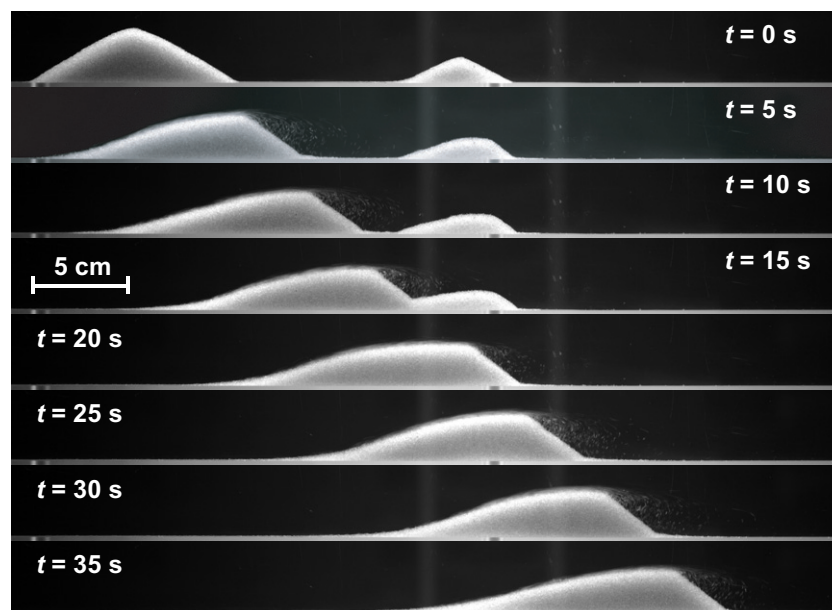


Figure 8. The development of the ‘large trailer’ as start configuration shown in analogy to figure 3.

between the two heaps is sufficiently long. At a short distance the small heap is located in the slipstream of the large heap. This scenario is shown in figure 8. Surprisingly, this ‘large trailer’ configuration also generates a barchan dune out of two smaller ones, similar to the small trailer configuration in figure 6.

The temporal evolution of the large trailer in figure 8 is shown in figure 9 as a stack plot of the height profiles. It is obvious that the water flow on the downwind side of the large heap is too weak to set the grains of the small heap in motion. Indeed the small heap is flattened but it

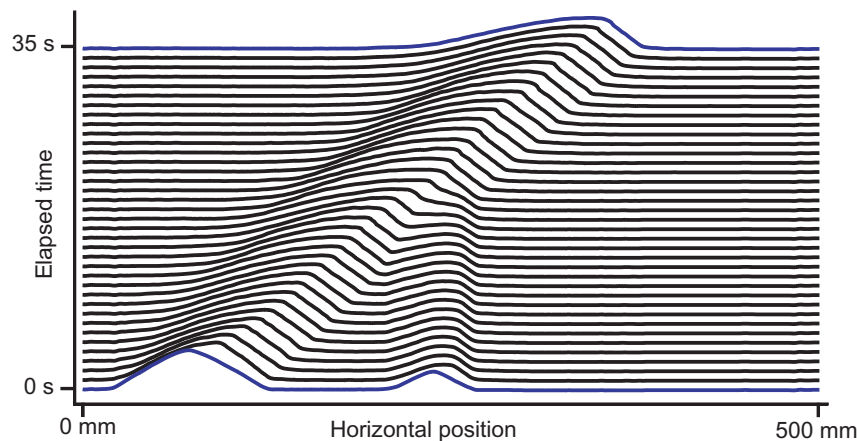


Figure 9. The temporal evolution of the height profile of the large trailer in figure 8 is shown as a stack plot. The time step is 1 s between each line. The starting profile and the final profile are marked blue (see movie 2, available from stacks.iop.org/NJP/11/023014/mmedia).

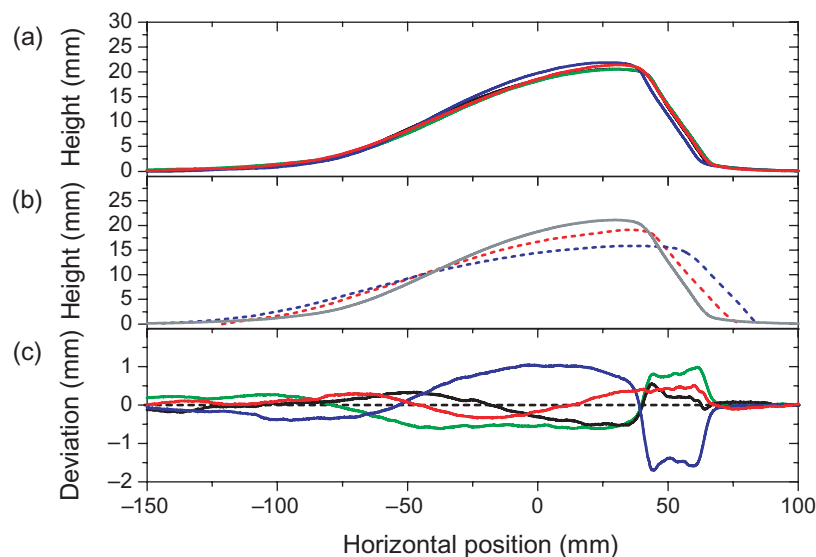


Figure 10. In panel (a), the averaged height profiles of the steady-state shapes of steep heap (red), flat heap (blue), small trailer (green) and large trailer (black) are shown in the centre-of-mass system. The shape of the attractor is shown as grey line in panel (b). Down-scaled barchan shape no. 1 (red dashed line) and no. 3 (blue dashed line) from the field data of [11] are shown in addition. The deviation of the averaged profiles from the mean shape profile is plotted in panel (c) with the colouring of panel (a).

rests in place until the large heap assimilates it. Like the small trailer, the large trailer acts like a dune with $m = 16.25$ g at the end of the collision process at $t = 20$ s.

In order to get the shape of the attractor, we average the steady-state shapes between $t = 35$ s and $t = 40$ s. In each case, we average 25 profiles in the centre-of-mass system. These averaged steady-state shapes for all four starting configurations are shown in figure 10(a).

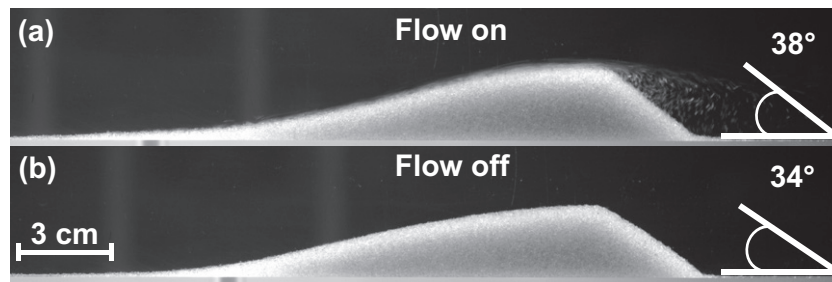


Figure 11. A study of the fully developed barchan dune with $m = 16.25$ g, $Re = 27\,000$. Snapshot (a) corresponds to the shape attractor in figure 10(b). For snapshot (b), the shearing water flow has been turned off. The slope of the slipface is indicated in each case.

We extract the shape of the attractor by averaging these four shapes. The result is shown in figure 10(b). The local deviation of the four averaged profiles from the attractor shape is plotted in figure 10(c). It is smaller than the three particle diameters.

The asymmetry of the shape attractor in figure 10(b) is primarily caused by the recirculation bubble on the leeward side [33]. This flow makes the slope at the downwind side even steeper than the angle of repose. This is illustrated in figure 11. If the shearing water flow is stopped, the recirculation bubble will disappear, and the slope of the slipface relaxes to its angle of repose at 34° . If the flow is turned on, the slope increases towards 38° , corresponding to the attractor shape. Moreover, it becomes apparent that the S-shape of the windward side is much less pronounced when the flow is turned off. This might explain why a parabolic approximation of this profile has been successful for data from field studies [11]. The length of the windward side and consequently the height of the dune depends on its mass and the flow velocity of the driving fluid [29].

From the field data in [11], we extracted the central shapes of two representative dunes, no. 1 and no. 3. We scale their area down to match that of the shape attractor found in our experiments. In figure 10(b), the scaled shapes are plotted as dashed lines together with the shape attractor in the centre-of-mass system. The scaling factors are 171 for dune no. 1 and 188 for dune no. 3, respectively. The shapes differ slightly, thus illustrating the effect that the attractor shape is not scale invariant. The characteristic asymmetry, however, is obvious in all cases. For aeolian dunes, the slope of the slipface has typical values between 31° and 35° [11], which is smaller than the subaqueous slope. Furthermore, the windward slope is more gradual in the aeolian cases. Both facts can partly be explained by the study illustrated in figure 11.

To get a quantitative measure of the four different relaxation processes towards the attractor shape, we use the root mean square deviation (RMSD) between the profiles of the barchan dunes and the attractor shape. The temporal evolution of the RMSD for all the four cases is shown in figure 12. The RMSD for the steep heap, the flat heap and the large trailer are decreasing functions, except for some fluctuations. The curve of the small trailer exhibits a noticeable plateau. Its end coincides with the merging of the two heaps (see figure 7).

All the four RMSD curves coincide quite well after $t = 35$ s. This means that after an adequate period, the four different starting configurations achieve the same shape attractor. This result is the experimental proof for the existence of a shape attractor for barchan dunes [24, 28].

The attractor is further characterized by its migration velocity. The temporal evolution of the four centre-of-mass velocities v_{com} is indicated in figure 13. The velocity v_{com} is determined

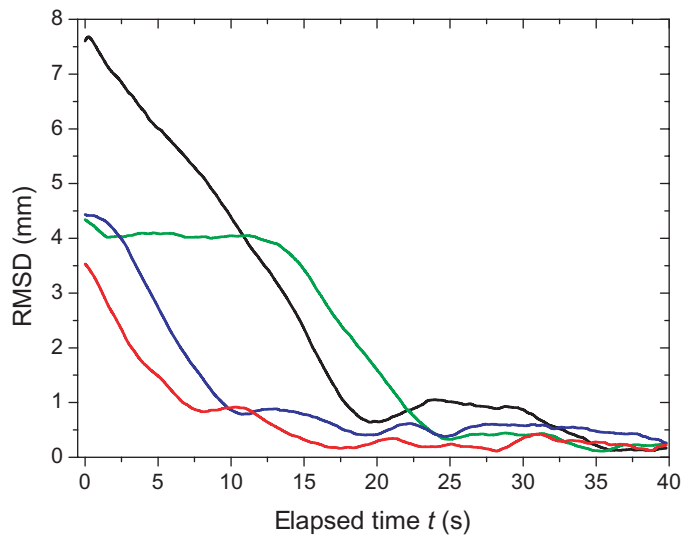


Figure 12. Temporal evolution of the RMSD between the shape profile and the mean steady-state shape profile for steep heap (red), flat heap (blue), small trailer (green) and large trailer (black).

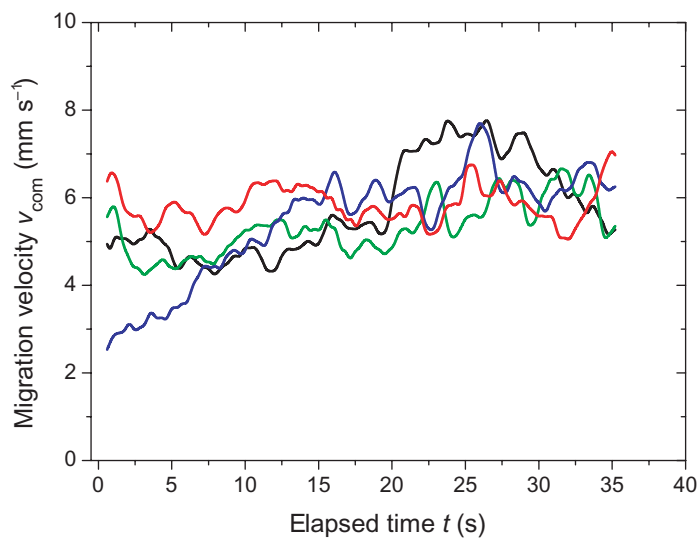


Figure 13. Temporal evolution of the centre-of-mass velocity v_{com} for steep heap configuration (red), flat heap configuration (blue), small trailer configuration (green) and large trailer configuration (black).

from the horizontal centre-of-mass displacement. The original data points are smoothed with a running average of 1 s. At the end of the measure time, the velocities achieve almost the same value, that is, the velocity of the shape attractor. Note that this velocity is only about one per cent of the flow velocity $v_{\text{flow}} = 0.45 \text{ m s}^{-1}$.

The difference of the aeolian dune shapes from the attractor shape in figure 10(b) indicates that the shape of the attractor depends on the flow velocity of the shearing medium and the size

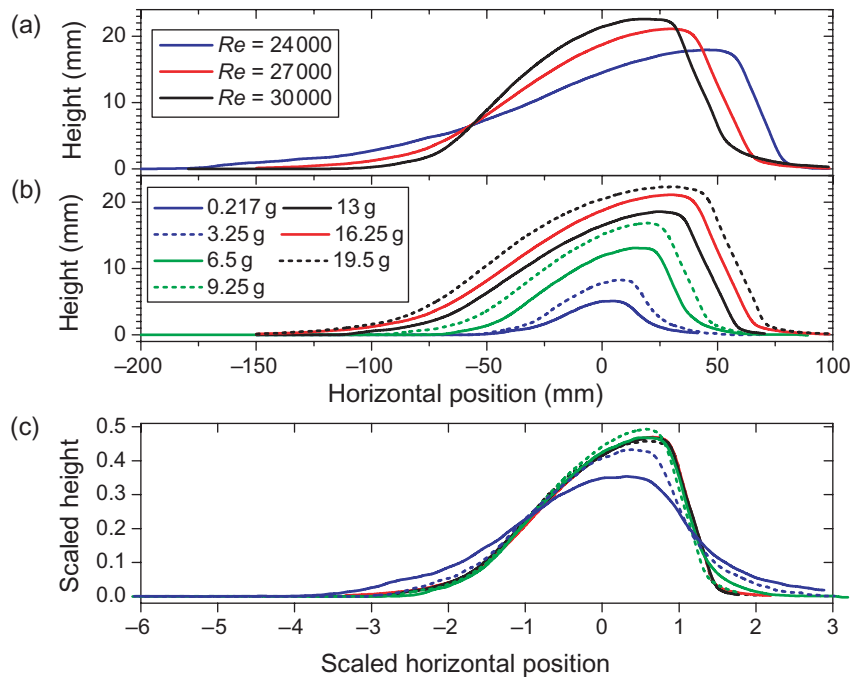


Figure 14. In panel (a), the shape of the attractor with $m = 16.25$ g is shown for the three different flow velocities. The attractor shapes for the seven different dune masses at a constant flow velocity corresponding to $Re = 27\,000$ are shown in panel (b) in the centre-of-mass system. In panel (c), these shapes are scaled by their cross section. The colour code in panels (b) and (c) is the same.

of the dune. To test the dependence on the flow velocity, we change the Reynolds number of the flow. Below $Re \approx 24\,000$, there is no clear dune migration, although some glass beads are in a slow creeping motion. The particles at the windward bottom, however, do not move. Above $Re \approx 30\,000$, the glass beads are sufficiently fast to leave the circulation bubble and to dart off. This leads to a mass loss and shrinking of the dune. The three attractor shapes for $Re = 24\,000$, $27\,000$ and $30\,000$ are plotted in figure 14(a). They indicate the dependence on the flow velocity: the larger the Reynolds number the steeper is the slope of the windward side. Notably, the slope of the slipface seems to be independent of the flow velocity.

To demonstrate the dependence of the shape attractor on the dune size, figure 14(b) shows the attractor shapes for seven different dune masses. The smallest dune has a mass of $m = 2.17$ g. For smaller masses, the height of the dune is below ten particle diameters, which would make the interpretation in terms of a continuum model questionable. For the largest dune, we choose $m = 19.5$ g, because larger dunes become unstable and decompose into several smaller dunes, which might be an effect of the finite channel height. For a better comparison of the different shapes, they are scaled with respect to their cross section A in figure 14(c), i.e. both the horizontal and the vertical axes are scaled by $1/\sqrt{A}$. Apparently, their slopes increase with increasing dune size, showing a tendency for saturation for masses larger than $m = 9.25$ g. This observation is in agreement with the literature [4, 6, 11, 24, 28, 29].

To conclude, we show the development towards a shape attractor on the basis of four different starting configurations in qualitative observation and quantitative analysis. A steep

heap becomes flatter and a flat heap becomes steeper until they both reach the shape attractor. The shape attraction also works if the initial topography is composed of two smaller dunes.

In the future, we want to investigate the dependence of the shape attractor on the grain size. Moreover, we feel that the investigation of the flow field will be of primary importance for the understanding of the barchan dune shape.

Acknowledgment

We are grateful for support from Deutsche Forschungsgemeinschaft through Kr1877/3-1 (Forschergruppe 608 ‘Nichtlineare Dynamik komplexer Kontinua’).

References

- [1] Pye K and Tsoar H 1990 *Aeolian Sand and Sand Dunes* (London: Unwin Hyman)
- [2] Lancaster N 1995 *Geomorphology of Desert Dunes* (London: Routledge)
- [3] Bagnold R A 1941 *The Physics of Blown Sand and Desert Dunes* (London: Chapman and Hall)
- [4] Andreotti B, Claudin P and Douady S 2002 Selection of dune shapes and velocities, part 2: a two-dimensional modelling *Eur. Phys. J. B* **28** 341–52
- [5] Kroy K, Sauermann G and Herrmann H J 2002 Minimal model for sand dunes *Phys. Rev. Lett.* **88** 054301
- [6] Kroy K, Sauermann G and Herrmann H J 2002 Minimal model for aeolian sand dunes *Phys. Rev. E* **66** 031302
- [7] Parteli E J R, Schwämmle V, Herrmann H J, Monteiro L H U and Maia L P 2006 Profile measurements and simulations of a transverse dune field in the Lençóis Maranhenses *Geomorphology* **81** 29–42
- [8] Hunt J C R, Leibovich S and Richards K J 1988 Turbulent shear flows over low hills *Q. J. R. Meteorol. Soc.* **114** 1435–70
- [9] Weng W S, Hunt J C R, Carruthers D J, Warren A, Wiggs C F S, Livingstone I and Castro I 1991 Air flow and sand transport over sand-dunes *Acta Mech. Suppl.* **2** 1–22
- [10] Sauermann G, Kroy K and Herrmann H J 2001 Continuum saltation model for sand dunes *Phys. Rev. E* **64** 031305
- [11] Sauermann G, Rognon P, Poliakov A and Herrmann H J 2000 The shape of the barchan dunes of southern Morocco *Geomorphology* **36** 47–62
- [12] Elbelrhiti H, Andreotti B and Claudin P 2005 Field evidence for surface-wave-induced instability of sand dunes *Nature* **437** 720–3
- [13] Elbelrhiti H, Andreotti B and Claudin P 2008 Barchan dune corridors: field characterization and investigation of control parameters *J. Geophys. Res.* **113** F02S15
- [14] White B R and Mounla H 1991 An experimental study of Froude number effect on wind-tunnel saltation *Acta Mech. Suppl.* **1** 145–57
- [15] Parteli E J R, Durán O and Herrmann H J 2007 Minimal size of a barchan dune *Phys. Rev. E* **75** 011301
- [16] Parteli E J R and Herrmann H J 2007 Saltation transport on Mars *Phys. Rev. Lett.* **98** 198001
- [17] Andreotti B, Claudin P and Douady S 2002 Selection of dune shapes and velocities, part 1: dynamics of sand, wind and barchans *Eur. Phys. J. B* **28** 321–39
- [18] Endo N, Taniguchi K and Katsuki A 2004 Observation of the whole process of interaction between barchans by flume experiments *Geophys. Res. Lett.* **31** L12503
- [19] Endo N, Sunamura T and Takimoto H 2005 Barchan ripples under unidirectional water flows in the laboratory: formation and planar morphology *Earth Surf. Process. Landforms* **30** 1675–82
- [20] Hersen P, Douady S and Andreotti B 2002 Relevant length scale of barchan dunes *Phys. Rev. Lett.* **89** 264301
- [21] Hersen P 2005 Flow effects on the morphology and dynamics of aeolian and subaqueous barchan dunes *J. Geophys. Res.* **110** F04S07
- [22] Andreotti B and Claudin P 2007 Comment on ‘minimal size of a barchan dune’ *Phys. Rev. E* **76** 063301

- [23] Charru F 2006 Selection of the ripple length on granular bed sheared by a liquid flow *Phys. Fluids* **18** 121508
- [24] Kroy K, Fischer S and Obermayer B 2005 The shape of barchan dunes *J. Phys.: Condens. Matter* **17** S1229
- [25] Parteli E J R, Durán O and Herrmann H J 2007 Reply to “comment on ‘minimal size of a barchan dune’” *Phys. Rev. E* **76** 063302
- [26] Taniguchi K and Endo N 2007 Deformed barchans under alternating flows: flume experiments and comparison with barchan dunes within Proctor Crater, Mars *Geomorphology* **90** 91–100
- [27] Schwämmle V and Herrmann H J 2003 Solitary wave behaviour of sand dunes *Nature* **426** 619
- [28] Fischer S, Cates M E and Kroy K 2008 Dynamic scaling of desert dunes *Phys. Rev. E* **77** 031302
- [29] Groh C, Wierschem A, Aksel N, Rehberg I and Krüelle C A 2008 Barchan dunes in two dimensions: experimental tests for minimal models *Phys. Rev. E* **78** 021304
- [30] Finkel H J 1959 The barchans of southern Peru *J. Geol.* **67** 614–47
- [31] Engelund F and Fredsøe J 1982 Sediment ripples and dunes *Annu. Rev. Fluid Mech.* **14** 13–37
- [32] Aguirre-Pe J, Olivero M L and Moncada A T 2003 Particle densimetric Froude number for estimating sediment transport *J. Hydraul. Eng.—ASCE* **129** 428–37
- [33] Ayrton H 1910 The origin and growth of ripple-mark *Proc. R. Soc. A* **84** 285